

Article

Elemental Enrichment in Shallow Subsurface Red Sea Coastal Sediments, Al-Shuaiba, Saudi Arabia: Natural vs. Anthropogenic Controls

Ibrahim M. Ghandour^{1,2,*}  and Mohammed H. Aljahdali¹

¹ Marine Geology Department, Faculty of Marine Sciences, King Abdulaziz University, Jeddah 80200, Saudi Arabia; maljahdli@kau.edu.sa

² Geology Department, Faculty of Science, Tanta University, Tanta 31527, Egypt

* Correspondence: ighandour@kau.edu.sa

Abstract: Geochemical analysis of the 23 sediment samples collected from a short (0.6 m long) core retrieved from the coastal creek that was previously connecting the northern and southern Al-Shuaiba Lagoons, Red Sea, Saudi Arabia, was accomplished to assess the elemental enrichment levels and the natural and anthropogenic driving forces for this enrichment. Statistical analysis and upcore variation in elemental concentrations enabled subdivision of the core formally into three units, lower, middle, and upper. The enriched elements in the lower and middle units display poor to negative correlations with the enriched elements in the upper unit. The lower unit is enriched in elements (Mo, As, U, and Re) suggesting deposition under anoxic conditions, possibly related to the Medieval Climate Anomaly. The middle unit is enriched in the carbonate-related constituents (CaCO₃, Ca, and Sr). The upper unit is enriched in elements that co-vary significantly with Al suggesting increased terrigenous supply associated with the construction of the road between the two lagoons. The enrichment of elements in the lower and middle units is naturally driven, whereas the enrichment of lithogenic elements in the upper unit, though of geogenic origin, is induced after the road construction.

Keywords: Al-Shuaiba Lagoon; anthropogenic vs. natural; Red Sea; sediment geochemistry; anoxic bottom conditions; redox-sensitive elements; terrigenous elements



Citation: Ghandour, I.M.; Aljahdali, M.H. Elemental Enrichment in Shallow Subsurface Red Sea Coastal Sediments, Al-Shuaiba, Saudi Arabia: Natural vs. Anthropogenic Controls. *Minerals* **2021**, *11*, 898. <https://doi.org/10.3390/min11080898>

Academic Editors: Marianna Kulkova and Dmitry Subetto

Received: 27 July 2021

Accepted: 17 August 2021

Published: 19 August 2021

Publisher's Note: MDPI stays neutral with regard to jurisdictional claims in published maps and institutional affiliations.



Copyright: © 2021 by the authors. Licensee MDPI, Basel, Switzerland. This article is an open access article distributed under the terms and conditions of the Creative Commons Attribution (CC BY) license (<https://creativecommons.org/licenses/by/4.0/>).

1. Introduction

Coastal lagoons are the most used, fragile, vulnerable, and threatened coastal ecosystems [1–5]. They hold varieties of important living resources of commercial and ecological interests. They are affected by several natural and anthropogenic pressures and threats. Climate changes, rock weathering, soil erosion, and volcanic eruptions are the most common natural threats. On the other hand, anthropogenic perturbations vary from various industrial and agricultural activities, burning of fossil fuels, untreated waste discharges, increasing nutrient supply, unplanned coastal urbanization, road runoff, dumping, and leachate from landfills [5–7]. These threats have a massive direct and indirect negative effect and increase the pressure on the marine coastal ecosystem. Water stagnation and poor flushing rates that are caused either by natural and/or anthropogenic processes are among the most serious environmental problems in coastal lagoons. Water stagnation puts pressure on the coastal water and sediment quality encourages the appearance of harmful algae and bacteria and eliminates oxygen from the ecosystem by anaerobic bacteria with the subsequent release of H₂S that can kill a variety of invertebrates and fishes and causes anomalous enrichment of the redox-sensitive metals [8]. Consequently, these coasts become unsuitable for aquaculture, fisheries, and coastal touristic and recreation activities.

The natural and anthropogenic threats and their environmental consequences are imprinted in the chemical composition of the lagoonal bottom sediments. These threats lead

to the enrichment of bottom sediments with potentially toxic elements. Metal enrichment can endanger aquatic life and destroy ecosystems [9,10]. The concentrations of trace elements in the sediments provide key information about potential anthropogenic pressures on the ecosystem, as well as potential internal sources in these ecosystems. Sediments are a possible source and/or a carrier for metals [11,12] and they may limit their bioavailability or allow their remobilization and re-suspension in the water column depending on bottom redox conditions [13,14]. Under certain conditions, the enriched toxic metals can be released into the water column and become a threat to aquatic ecosystems as well as a health risk to humans due to their toxicity, persistence, and ability to accumulate in living organisms [5,15,16]. Therefore, the study of sediment geochemistry is crucial to monitor the aquatic ecosystem as it provides information about the redox bottom conditions, contamination level, and ecotoxicological risk [5,17]. The chemical composition of shallow subsurface coastal sediments provides a historic record of natural and anthropogenic influences on coastal systems [18–20].

Along the Saudi Red Sea coast, there are over 20 hypersaline coastal lagoons with unique environmental characteristics [21]. Among them, Al-Shuaiba and Al-Kharrar Lagoons are the most studied [22–27]. At Al-Shuaiba area some 80 km south of Jeddah City, there are two lagoons, the northern and southern Al-Shuaiba Lagoons (Figure 1a), that are sites for rare traditional fishing. In the past, water was freely circulated between the two lagoons through a shallow and small channel/creek and the oxygen concentration in the water was normally replenished. In the early 1980s, the two lagoons were separated by a paved road, which ended water circulation and the area has undergone dramatic environmental changes (Figure 2). Water circulation in the channel to the north of the southern Al-Shuaiba Lagoon is sluggish and essentially stagnant, resulting in the accumulation of organic matter from dead organisms and plants from the nearby mangroves.

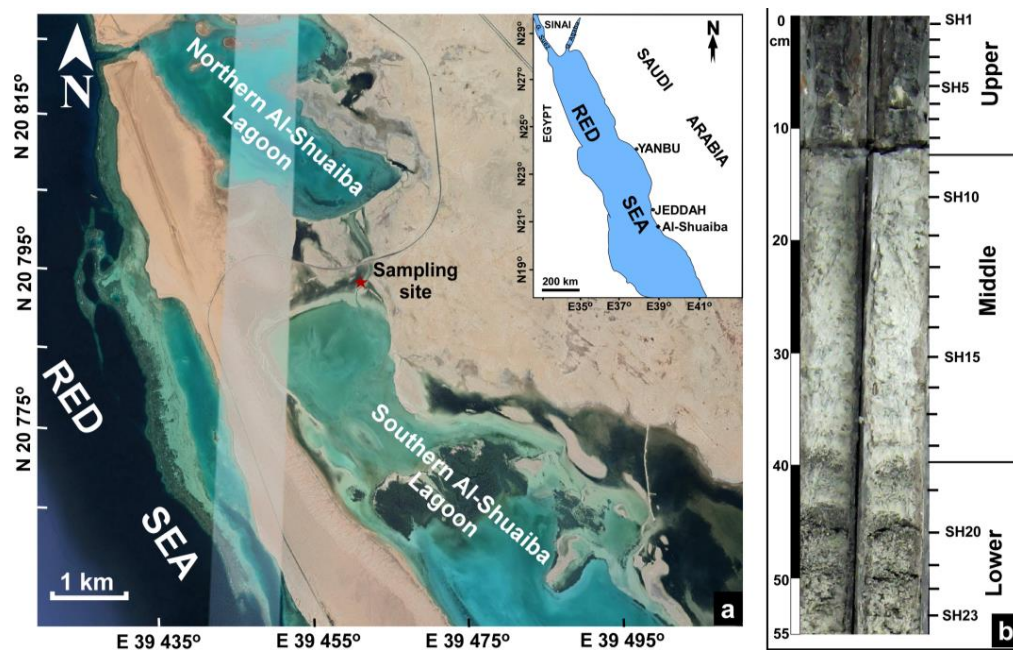


Figure 1. Location map of the area of study (a) and the core sample (b).

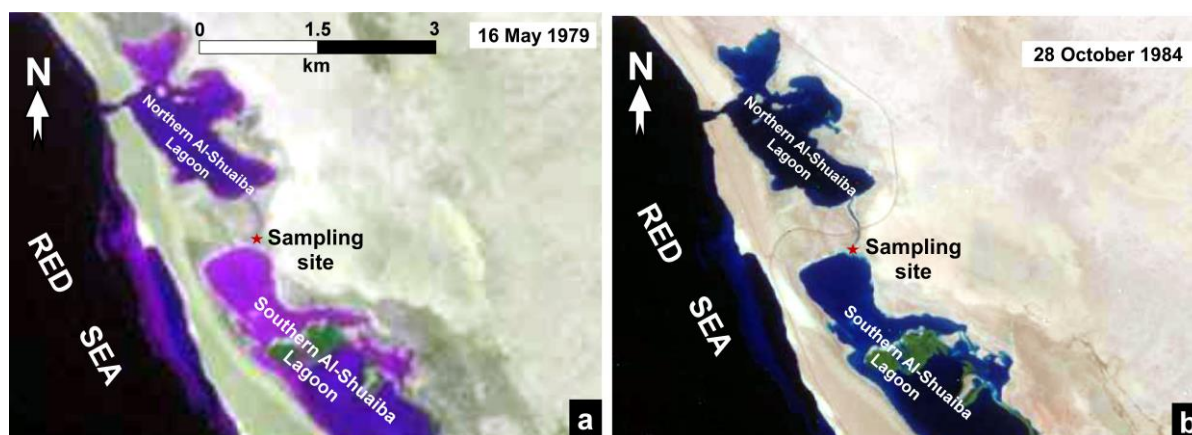


Figure 2. Historic land-sat images of Al-Shuaiba area showing the evolution of the area before (a) and after the road construction (b) between the two lagoons.

Most of the previous studies in the Al-Shuaiba area were carried out on the southern Al-Shuaiba Lagoon bottom sediments and the shallow subsurface sediments of the tidal flat to the east. The effect of meteorological forcing and tide on the flushing of Al-Shuaiba Lagoon was studied by Ahmad and Sultan [28] and Al-Barakati [29]. The mineralogical and chemical composition of the southern Al-Shuaiba Lagoon bottom sediment was studied by Al-Washmi and Gheith [22] and Basaham et al. [26], whereas Abu-Zied and Bantan [24] studied the benthic foraminiferal distribution and their environmental controls and usefulness in sea-level reconstruction. Abu-Zied and Bantan [30] studied the vertical variations of benthic foraminifera and major and trace elements and their environmental and paleoclimatic significances in shallow subsurface sediments of the tidal flat east of the southern Al-Shuaiba Lagoon. Al-Farawati et al. [31] studied the speciation and distribution pattern of phosphorus in the sediments of the northern Al-Shuaiba Lagoon.

None of the previous studies has committed an investigative effort to document the potential impacts of road construction on the water and sediment quality of the area. The environmental deterioration and adverse effect of road construction on sediment chemical composition are therefore a target of this work. It is crucial to determine sediment geochemistry and assess if any metal enrichment has been caused or amplified by the construction of the road in the early 1980s and the resultant stagnation. The present work, therefore, aims to (1) reveal the vertical profiles and assess the degree of enrichment of the environmentally sensitive major and trace elements prior to and after the construction of the road; (2) determine the reason(s) and sources of elemental enrichment; and (3) evaluate the most suitable redox-sensitive elements. To investigate the history of the channel and the beginning of the anthropo-pressure, coring of the bottom sediments of the channel/creek connecting the two lagoons was conducted.

2. Area of Study

The northern and southern Al-Shuaiba Red Sea hyper-saline coastal lagoons (Figure 1a) were formed by the sub-pluvial to pluvial Pleistocene erosion and subsequently submerged by a sea-level rise during the early-middle Holocene [21,32,33]. They are bounded to the west by raised coral terraces of Pleistocene age and the east by a vast tidal flat. They show unique environmental characteristics as they are connected to the Red Sea through narrow inlets with water depths of 7 and 15 m, respectively. The climate is tropical with warm and dry conditions throughout the year, scarce rainfall (63 m/year), and no riverine inflow. The annual average evaporation rate over the Red Sea is 2.06 ± 0.22 m/year [34,35].

The lagoons are separated by a paved road that ended the water circulation. They lack industrial, freshwater, and terrigenous sediments influx. The lagoonal bottom sediments consist of calcareous biogenous sediments admixed with relatively rare siliciclastic and traces of evaporite deposits [21]. The texture of the bottom sediments ranges between sandy

mud and gravelly sand. The sand to gravel size fraction is dominated by skeletal remains of coral debris, coralline algae, molluscan shells, foraminifera, sponges, and bryozoans. The sediment distribution is controlled by the shape and size of the inlet, water depths, and tidal currents. The colour of sediments varies in the two lagoons, with dark sediments mainly found at the periphery of the lagoons. The bottom sediments of the northern lagoon are brown to grey, whereas they range from yellow to grey in the southern lagoon. Fine sediments are dark with shades of grey, and the coarse sediments are light with shades of yellowish to greyish brown. The coarse sediments including shells are stained grey to black due to the reducing environment and formation of authigenic pyrite. Stagnant conditions prevail inside the lagoons due to insufficient water exchange with the open sea, and the lack of rainfall causes hyper-saline conditions [21]. Dark grey sediments occur in quiescent reducing areas where currents are almost negligible and incapable of re-suspending and transporting sediments. The reducing environment is further enhanced by restricted water exchange between the Red Sea and the lagoons. Organic-rich sediments with a pungent smell are dark-coloured and enriched in mangrove and dark stained shells and coral debris remains reflecting the development of reducing conditions [21].

Basaham et al. [26] distinguished two groups of elements in the southern Al-Shuaiba lagoonal bottom sediments. The first group defines elements that are associated with detrital minerals such as silicates (Al-Fe-Si), feldspars (K-Rb-Ba), and heavy minerals (V-Cr-Zr, Ti-Y-Nb). They are highly enriched in the shallow nearshore sediments. The second group defines elements Ca and Sr that are associated with carbonate minerals and are concentrated in the deeper parts of the lagoon. Mangrove (*Avicennia marina*) stands are scattered around the small islands and along the eastern margins of the lagoons. Seagrass and macro-algae dominate the shallow parts of the lagoons [36]. Abu-Zied and Bantan [30] recorded benthic foraminiferal assemblages, *Monalysidium acicularis*, *Quinqueloculina* cf. *Q. limbata*, and *Coscinospira hemprichii* that are sensitive indicators of sea-level changes.

3. Materials and Methods

A short core (0.6 m long) was obtained by simple manual push and rotation from the channel that connects the two Al-Shuaiba Lagoons in a water depth of 0.6 m. The core was collected by a simple manual push with rotation using a PVC tube with a 6.35 cm internal diameter. Twenty-three samples were collected from the upper 0.55 m at 1.5 to 2-cm sampling intervals (Figure 1b). Dissolved oxygen (DO), water salinity, and pH were measured for the surface water, sediment-water interface, and interstitial waters using a handheld multi-parameters instrument YSI 556 MPS (YSI Environmental, Yellow Springs, OH, USA). The samples were dried at room temperature then at 105 °C for 24 h to remove water. The concentrations of major (>1%), minor (between 1% and 100 µg/g), and trace (equal to or below 100 µg/g) were performed using the multi-acid digestion package ICP-ES/MS (MA200) at the Bureau Veritas Mineral Laboratories (BVML, Vancouver, Canada). A 0.25 g of the sample was heated in HNO₃, HClO₄, and HF to fuming and taken to dryness. The residue was then dissolved in HCl. The concentrations of elements were determined using the ICP-MS with a Perkin Elmer Elan 6000 ICP (Perkin Elmer, Waltham, MA, United States) mass spectrometer and the concentrations were expressed as µg/g. Procedural blanks and certified reference materials OREAS 25A-4A and OREAS 45E were prepared using the same analytical procedure and reagents and analyzed for the BVML quality assurance/control (QA/QC) protocol. Organic matter content was determined by loss of weight by ignition (LOI₅₅₀) in a muffle furnace at 550 °C for 2 h [37]. To assess the possible elemental enrichments, the enrichment factor (EF; [38]) is determined as follows:

$$EF = ([X]/[R])_{sample} / ([X]/[R])_{reference}$$

where X is the concentration of an element and R is the concentration of the normalizer. The reference material used in this study is local reference corresponding to uncontaminated sediments in the same core. It represents the average chemical composition of three samples from the core assumed to correspond to sediments deposited prior to the

complete closure of the canal. Since it is conservative and of natural origin, titanium (Ti) was chosen as a normalizer. Ti is contributed mainly by and is located entirely in heavy and clay minerals. Five categories of enrichments are defined [39]: $EF < 1.5$ no enrichment; $1.5 < EF < 5$ moderate; $5 < EF < 20$ significant; $20 < EF < 40$ very high; and $EF > 40$ extreme. In addition, the data of some elements were also normalized against the most abundant lithogenic element—aluminum (Al). Pearson correlation and multivariate analysis were performed using IBM SPSS Statistics for Windows, Version 20.0. (IBM Corp., Armonk, NY, USA). The principal component analysis (PCA) was used to determine relationships among variables and simplify the analytical dataset. The sample matrix consists of 23 sediment samples and 30 variables.

4. Results

The water salinity, pH, and dissolved oxygen (DO) vary in the channel with depth. The surface water salinity, pH, and DO are 51.56‰, 8.4 and 6.08 mg/L, respectively, and they are 39.1‰, 8.08 and 1.92 mg/L, respectively, at the sediment-water interface. A remarkable decrease in salinity (28.88‰), pH (8.01), and DO (0.51 mg/L) is recorded for the interstitial waters.

Based on the colour, sediment composition, texture and organic matter, CaCO_3 , and elemental concentrations, the core sediments can be subdivided into three units, upper, middle, and lower (Figure 1b). The upper unit spans the top 12 cm, marked by dark grey to black colour with stench smell. It consists of argillaceous sands with abundant algal mats. The middle unit extends from 12 to 39 cm and consists of light grey to white calcareous sands enriched in molluscan shell fragments. The lower unit extends from depths 39 to 55 cm and it consists of colour banded, massively bedded, light grey sands (Figure 1b).

4.1. Chemical Composition

The elemental concentrations and their enrichment factors, LOI_{550} , and CaCO_3 contents of 23 samples are summarized in Table 1 and the down-core variations of their concentrations are shown in Figure 3. The geochemical composition of the sediments shows a downcore co-variation of elements Al, Fe, Mg, K, Na, P, LOI_{550} , Mn, V, Cr, Co, Ni, Zn, Zr, Rb, La, Li, Nb, Sc, and Ce. Their concentrations are higher in the upper than the middle and lower parts of the core (Figure 3). The downcore distribution pattern of these elements shows an opposite trend to Ca, Sr, CaCO_3 , Mo, As, U, and Re (Figure 3). The value of the LOI_{550} increases monotonically upcore with the highest content in the upper unit which contains the highest proportion of terrigenous mud. It varies from 3% to 15% (mean 9%). The CaCO_3 decreases upcore ranging from 75% to 36% (mean 59%). On average, the most abundant major elements are Ca (22.95%), Mg (2.9%), Al (2.48%), Na (1.51%), and Fe (1.34%). Ca varies in the lower and middle parts of the core between 23.65% and 27.09%, whereas it varies in the upper part from 14.55% to 20.51%. The Al content varies in the lower and middle parts of the core from 1.62% to 2.66%, whereas it ranges between 3.11% and 4.19% in the upper part. Similarly, the highest concentrations of Mg (4.45%), Na (2.33%), and Fe (2.09%) were recorded from the upper part of the core (Figure 3).

Table 1. Results of chemical analysis of the shallow subsurface coastal sediments of the creek that was connecting the two Al-Shuaiba Lagoons. Ranges and average (in brackets) of concentrations, enrichment factor (EF), Al-normalized elements, and the calculated background values.

Element/ Constituent	Concentrations	Enrichment Factor	Al-Normalized	Background Values
Ti%	0.14–0.33 (0.21)	-	0.059–0.173 (0.090)	0.215
Al%	1.62–4.19 (2.48)	-	-	2.15
Fe%	0.81–2.09 (1.34)	0.62–1.72 (1.19)	0.497–0.590 (0.543)	1.17
Ca%	14.55–27.09 (22.95)	0.47–1.55 (0.98)	3.473–16.722 (10.292)	24.95
Mg%	1.95–4.45 (2.9)	0.61–1.71 (1.20)	0.942–1.484 (1.199)	2.53
Na%	0.83–2.33 (1.51)	0.66–1.97 (1.21)	0.441–0.778 (0.620)	1.3
K%	0.43–0.96 (0.59)	0.63–1.55 (1.18)	0.213–0.340 (0.245)	0.53
P%	0.03–0.05 (0.04)	0.68–1.51 (1.18)	0.013–0.019 (0.016)	0.033
S%	0.3–0.6 (0.44)	0.54–1.80 (1.28)	0.095–0.227 (0.185)	0.37
CaCO ₃ %	36–75 (59)	-	-	-
LOI ₅₅₀ %	3–15 (9)	-	-	-
Mn µg/g	153–405 (264)	0.79–1.39 (1.11)	93.67–156.91 (108.99)	245
V µg/g	25–70 (42)	0.68–1.60 (1.18)	15.43–20.22 (17.11)	36.7
Cr µg/g	15–44 (26.96)	0.67–1.83 (1.29)	9.26–14.07 (10.97)	21.7
Co µg/g	1.9–11.2 (5.45)	0.51–2.23 (1.30)	1.17–2.69 (2.10)	4.3
Ni µg/g	4.2–22.9 (12.54)	0.54–2.37 (1.37)	2.59–6.59 (4.84)	9.4
Cu µg/g	5.30–24 (11.07)	0.53–3.15 (1.47)	3.14–8.47 (4.36)	7.8
Zn µg/g	9–49 (24.6)	0.58–2.95 (1.49)	5.56–14.85 (9.41)	17
Pb µg/g	2.7–24.6 (10.13)	0.26–2.82 (1.24)	1.47–12.36 (4.08)	8.5
Zr µg/g	8.5–30.7 (19.72)	0.63–1.59 (1.10)	5.25–9.79 (7.98)	18.5
Ce µg/g	10–22 (15.3)	0.60–1.29 (1.04)	5.06–7.91 (6.34)	15.3
Nb µg/g	1.9–4.6 (3.12)	0.83–1.45 (1.12)	1.04–2.02 (1.30)	2.87
Rb µg/g	11.9–26.5 (16.87)	0.59–1.60 (1.19)	6.32–7.96 (6.87)	14.8
La µg/g	5.2–11 (7.7)	0.59–1.25 (1.00)	2.53–4.05 (3.19)	8
Y µg/g	4.5–11.7 (7.43)	0.74–1.42 (1.12)	2.69–4.20 (3.06)	6.87
Sc µg/g	2–9 (5.09)	0.66–1.93 (1.32)	1.23–2.31 (2.04)	4
Li µg/g	4–13.6 (8.21)	0.56–1.89 (1.25)	2.47–3.92 (3.28)	6.8
Sr µg/g	1618–3957 (3201)	0.36–1.32 (0.93)	386.16–2043.83 (1416.84)	3631
Sb µg/g	0.3–2.7 (0.63)	0.72–5.97 (1.75)	0.12–0.64 (0.24)	0.37
Sn µg/g	0.2–2.6 (0.64)	0.46–6.25 (1.54)	0.12–0.83 (0.24)	0.43
Th µg/g	0.8–3.2 (1.49)	0.69–1.51 (1.08)	0.44–1.70 (0.62)	1.4
Mo µg/g	2.1–7.5 (4.83)	0.45–3.10 (1.64)	0.67–4.44 (2.09)	3.2
As µg/g	5–17 (9.35)	0.81–3.34 (1.61)	1.91–9.04 (4.25)	6.3
U µg/g	3.2–8 (5.34)	0.57–2.55 (1.26)	0.76–4.55 (2.40)	4.6
Re µg/g	0.003–0.035 (0.013)	0.19–4.45 (1.38)	0.0007–0.0188 (0.0060)	0.01

The most abundant trace elements in the sediments are Sr (mean 3201 µg/g) and Mn (mean 264 µg/g), whereas other trace elements occur in concentrations less than 100 µg/g (Table 1). Compared with the samples in the middle and lower units, the samples of the upper unit contain relatively high trace element content except for Mo, As, U, and Re (Figure 3). The concentration ranges of V, Cr, Co, Ni, Cu, and Zn are 25–70, 15–44, 1.9–11.2, 4.2–22.9, 5.30–24, and 9–49 µg/g, respectively (Table 1). Trends for Mo, As, U, and Re are all characterized by pronounced positive peaks marking the lower part of the core (Figure 3), corresponding to the low concentrations of other trace elements. Although the overall concentration of Cu and Zn increases upcore, the highest concentrations of the two elements appear at 7–9 cm depth (Figure 3). Lead (Pb) showed irregular variations compared with the other heavy metals (Figure 3). Sb and Sn were relatively constant in the lower part of the core and increased markedly at the depths of 3 and 6 cm, respectively (Figure 3). A clear upcore change in Al-normalized trace elements is apparent. A significant feature of the upper part is the remarkable enrichment in Al-normalized concentrations of Co, Ni, and Zn, whereas the lower part notably shows enrichment in Al-normalized Mo, As, U, and Re (Figure 4). The profiles of Al-normalized Mn and V are relatively similar showing peaks in the middle unit (Figure 4).

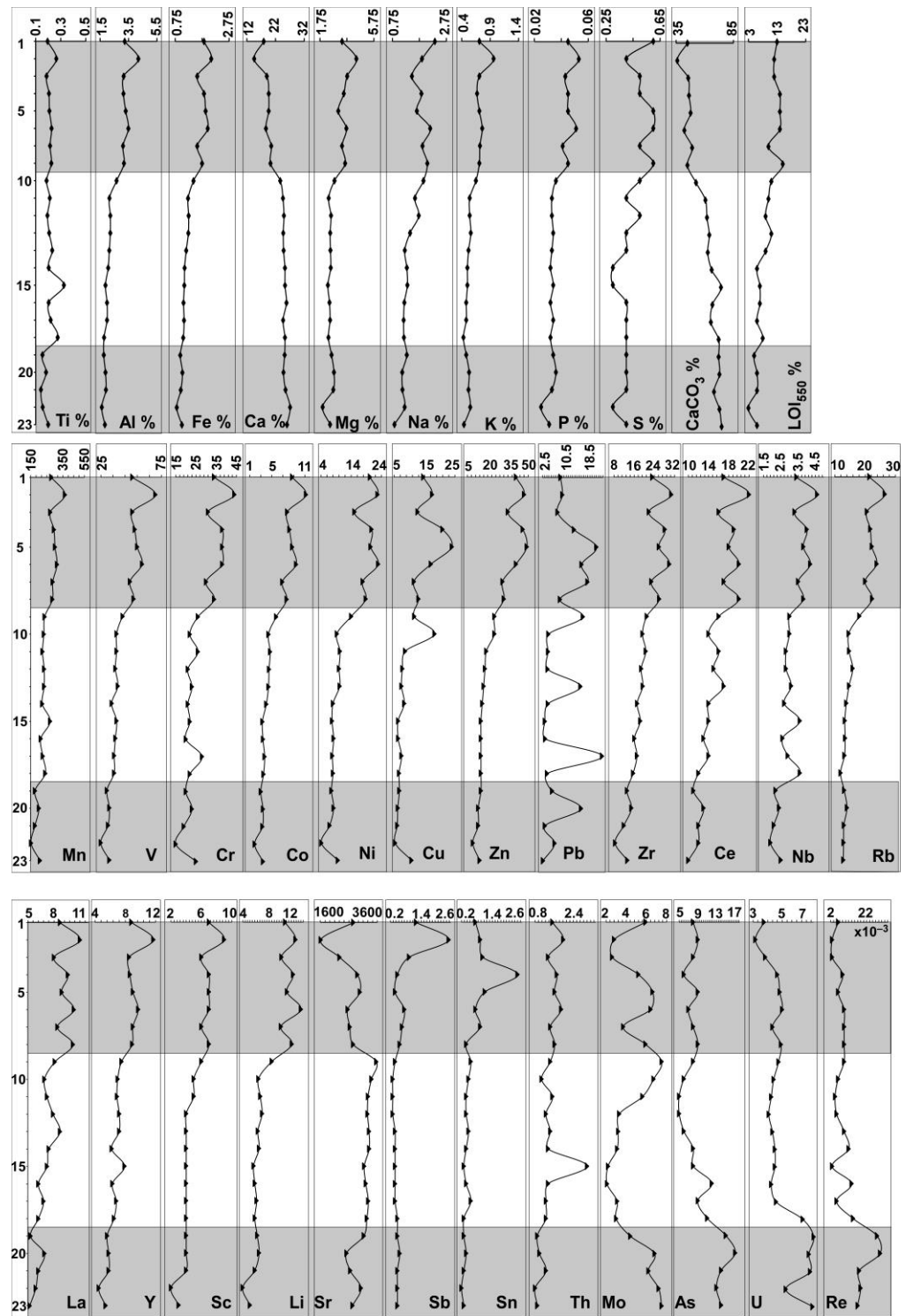


Figure 3. The upcore variation in the concentrations of major (%) and trace elements ($\mu\text{g/g}$). Elements Al, Fe, Mg, K, Na, OM, Mn, V, Cr, Co, Ni, Zn, Zr, Ce, Nb, Rb La, Y, Li, and Sc display the same profile enriched in the upper unit, Ca, CaCO_3 , and Sr behave similarly and Mo, As, U, and Re show similar vertical distribution pattern.

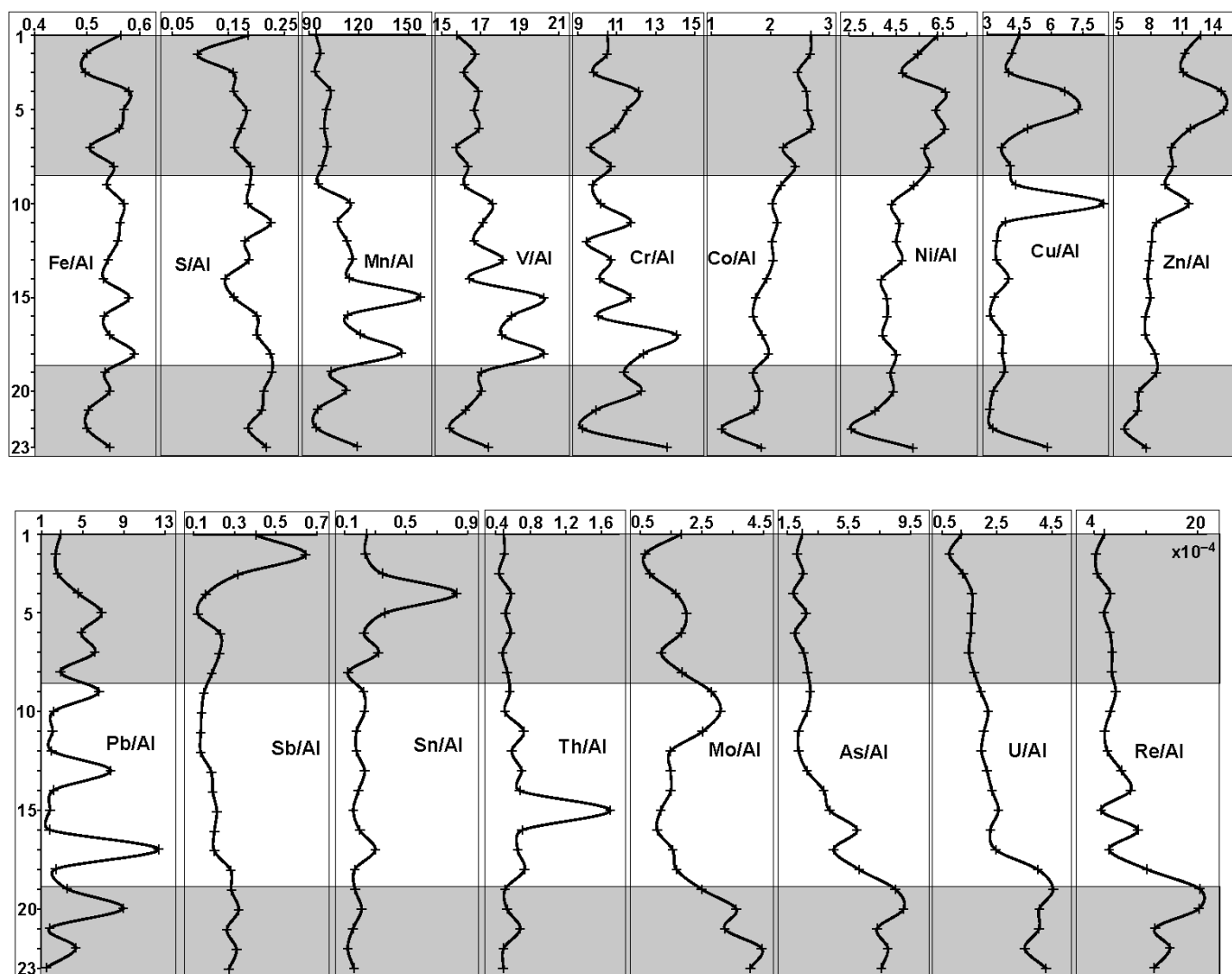


Figure 4. The vertical profiles of Al-normalized elements. Note the upcore increase in the Al-normalized Co, Ni, and Zn values, and the upcore decrease in the Mo/Al, As/Al, U/Al, and Re/Al values. Values of minor and trace elements are multiplied by 10^{-4} .

Aluminum (Al) shows a significant positive correlation ($r \geq 0.9$) with Fe, Mg, K, P, Mn, V, Cr, Co, Ni, Zn, Zr, Ce, Rb, La, Y, Sc, and Li (Table 2). It correlates positively with OM ($r = 0.86$), Na ($r = 0.8$), Nb ($r = 0.82$), and Cu ($r = 0.78$). The significant positive correlations between Al and trace elements Mn, V, Cr, Co, Ni, Cu, and Zn (Figure 5) implies that these elements were derived from a terrigenous source and were not measurably enhanced by reduction from the water column. On the other hand, Ca shows a significant positive interrelationship with CaCO_3 ($r = 0.94$) and Sr ($r = 0.7$). These three components negatively correlated with elements characteristic of the detrital fraction (Table 2), suggesting that they are present in the carbonate fraction. Trace elements Mo, As, U, and Re correlate negatively ($r \leq 0$) with Al (Table 2). The significant positive correlation between Ti and Th ($r = 0.75$) indicates detrital fluxes and most Th is held in clay and heavy minerals [40,41].

Table 2. Pearson correlation matrix between Ti, Al, Fe, Ca, CaCO₃, and LOI₅₅₀ and major, minor, and trace elements in the shallow subsurface coastal sediments of the creek that was connected with the two Al-Shuaiba Lagoons.

Element/ Constituent	Ti	Al	Fe	Ca	CaCO ₃	LOI ₅₅₀
Ti	1.00	-	-	-	-	-
Al	0.19	1.00	-	-	-	-
Fe	0.24	0.98 **	1.00	-	-	-
Ca	-0.20	-0.98 **	-0.96 **	1.00	-	-
Mg	0.13	0.94 **	0.89 **	-0.96 **	-	-
Na	0.10	0.81 **	0.85 **	-0.77 **	-	-
K	0.12	0.96 **	0.91 **	-0.94 **	-	-
P	0.24	0.95 **	0.96 **	-0.97 **	-	-
S	-0.10	0.7 **	0.76 **	-0.67 **	-	-
CaCO ₃	-0.11	-0.98 **	-0.96 **	0.94 **	1.00	-
LOI ₅₅₀	0.24	0.86 **	0.92 **	-0.81 **	-0.88 **	1.00
Mn	0.58 **	0.9 **	0.92 **	-0.89 **	-0.84 **	0.83 **
V	0.36	0.98 **	0.98 **	-0.96 **	-0.94 **	0.86 **
Cr	0.28	0.93 **	0.95 **	-0.94 **	-0.89 **	0.82 **
Co	0.21	0.99 **	0.99 **	-0.98 **	-0.97 **	0.88 **
Ni	0.20	0.97 **	0.99 **	-0.94 **	-0.94 **	0.9 **
Cu	0.11	0.78 **	0.84 **	-0.75 **	-0.77 **	0.8 **
Zn	0.17	0.94 **	0.97 **	-0.94 **	-0.93 **	0.88 **
Zr	0.39	0.92 **	0.96 **	-0.88 **	-0.91 **	0.91 **
Ce	0.32	0.91 **	0.92 **	-0.85 **	-0.91 **	0.85 **
Nb	0.67 **	0.82 **	0.86 **	-0.82 **	-0.77 **	0.80 **
Rb	0.15	0.99 **	0.98 **	-0.96 **	-0.97 **	0.87 **
La	0.34	0.9 **	0.91 **	-0.85 **	-0.89 **	0.86 **
Y	0.47 *	0.94 **	0.94 **	-0.93 **	-0.9 **	0.83 **
Sc	0.23	0.96 **	0.97 **	-0.95 **	-0.95 **	0.87 **
Li	0.16	0.96 **	0.97 **	-0.94 **	-0.95 **	0.9 **
Sr	-0.04	-0.6 **	-0.52 *	0.7 **	0.50 *	-0.29
Sb	0.21	0.68 **	0.59 **	-0.75 **	-0.59 **	0.32
Sn	0.04	0.63 **	0.67 **	-0.64 **	-0.64 **	0.61 **
Pb	0.01	0.4	0.41	-0.37	-0.42 *	0.33
Th	0.75 **	0.43 *	0.47 *	-0.41	-0.36	0.42 *
Mo	-0.5 *	0.00	0.05	0.04	-0.04	0.08
As	-0.38	-0.43 *	-0.49 *	0.34	0.51 *	-0.61 **
U	-0.35	-0.57 **	-0.55 **	0.51 *	0.61 **	-0.51 *
Re	-0.5 *	-0.5 **	-0.55 **	0.47 *	0.56 **	-0.59 **

Note: ** Correlation is significant at the 0.01 level; *correlation is significant at the 0.05 level.

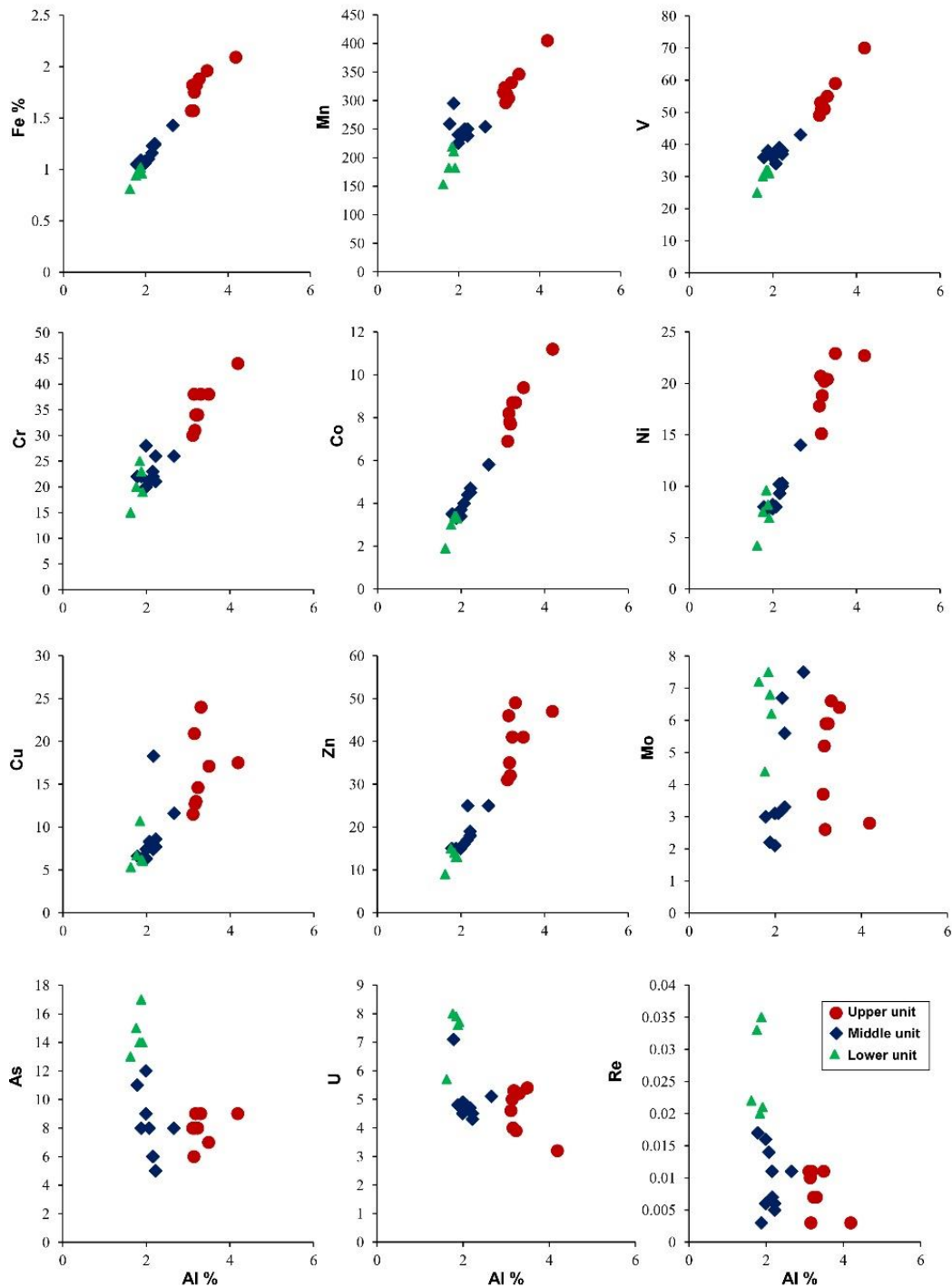


Figure 5. Bivariate plots between Al (%) and major (Fe %), minor (Mn) and trace elements V, Cr, Co, Ni, Cu, Zn, Mo, As, U, and Re ($\mu\text{g/g}$). Note the positive correlation with the first eight elements and the poor and negative correlation with the last four elements.

4.2. Enrichment Factor

The enrichment factors (*EF*) for Fe, Mn, V, Cr, Co, Ni, Cu, Zn, Mo, As, U, and Re were calculated using the average concentration of local background and Ti as a normalizer. The *EF* values are shown in Table 1 and the vertical profiles for some trace elements are displayed in Figure 6. Most trace elements are depleted relative to the average local background, except for Mo, U, As, and Re in the lower unit. Elements Fe, Mn, V, Cr,

Co, Ni, Cu, and Zn are generally depleted in the lower and middle units of the core, whereas Fe, V, Cr, Co, Ni, Cu, and Zn are slightly enriched ($1.5 < EF < 5$) in the upper unit (Figure 6). Manganese (Mn), Sb, and Sn are below the local background level ($EF < 1.5$). However, some samples in the upper unit show slight to moderate enrichment for Sb and Sn ($1.5 < EF < 10$). Some samples in the lower and upper parts show slight enrichment of Pb ($1.5 < EF < 5$). The lower part shows slight enrichment ($1.5 < EF < 5$) of Mo, As, U, and Re, whereas As, U, and Re are depleted in the middle and upper parts of the core (Figure 6).

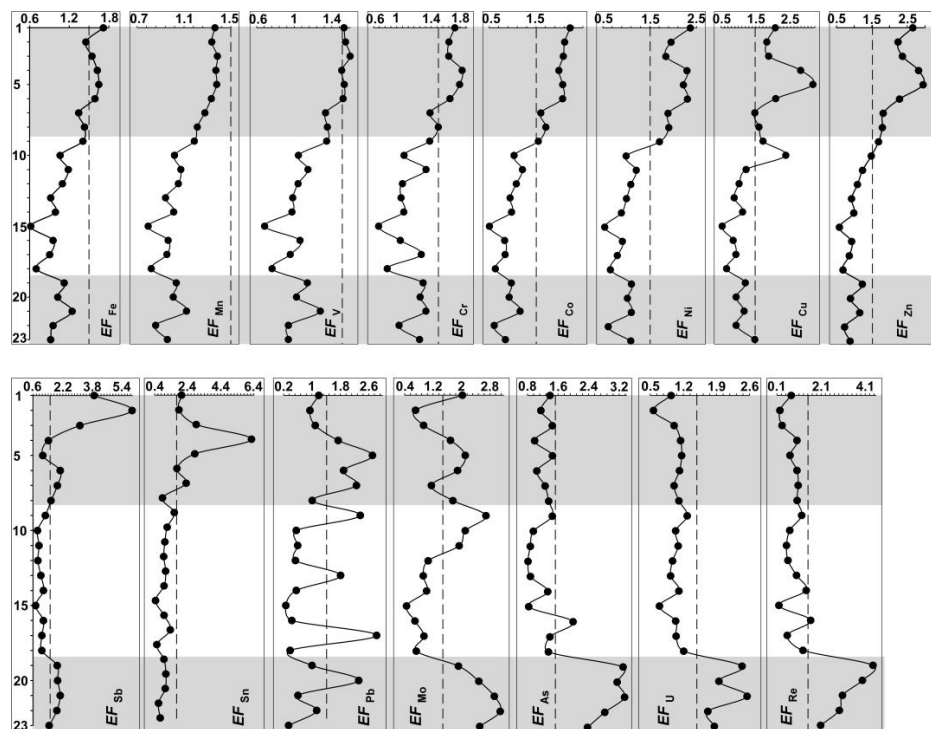


Figure 6. The vertical profile of *EF* values of environmentally significant major (Fe), minor (Mn), and trace elements. The *EF* values for Cr, Co, Ni, Cu, and Zn are slightly enriched in the upper unit, whereas the lower unit shows higher *EF* values for Mo, As, U, and Re than the other two units.

4.3. Statistical Analysis

To determine the similarities and differences between sampling sites and to identify a potential source(s) of elements and the controlling factors on their concentration and distribution, the geochemical dataset was treated statistically using principal component analysis (PCA). The matrix includes 23 sediment samples and 30 variables. Components with eigenvalues greater than 1 were retained. The positive higher loadings of elements were used for factor interpretations.

Four components, with eigenvalues greater than 1, account for 89.28% of the total variance (Table 3). The first two components explain 68% and 10.67% of the total variance, respectively, and thus, account for most of the variance. Components 3 and 4 explaining 7.03% and 3.58% are less important. According to the loadings of components 1 and 2, elements can be roughly clustered into three primary groups. Component 1 is characterized by positive scores (>0.9) for lithogenic constituents (Fe, V, Co, Al, Zr, Y, Ni, Rb, Sc, Zn, Cr, P, Mn, Ce, Nb, and LOI_{550}). These elements are enriched in the sediments of the upper unit. Component 2 characterizes hydrogenous elements (Mo, As, U, and Re as the main positive descriptors) and corresponds to the sediments of the lower unit (Figure 7a). The elements Mo, As, U, and Re are projected in the quadrant of negative values of component 1 and positive values of component 2, while calcareous biogenic components (Ca, $CaCO_3$, and Sr) are in an adjacent quadrant with negative values for components 1 and 2. Elements Ti

and Th are clustered into one group indicating their possible similar source and behaviour. They are projected in the quadrant with positive values of component 1 and negative values of component 2. Elements Nb, Mn, Y, Zr, Ce, and V are projected in the quadrant of positive values of component 1 and negative values of component 2 (Figure 7a). The rest of the metals (Cu, Pb, Sb, and Sn) are gathered together and may indicate another possible anthropogenic source.

Table 3. Results of principal component (R-mode) analysis, four components (PC1-PC4) extracted with the PC1 and PC2 are the most important. Significant values are in bold.

Variable	PC1	PC2	PC3	PC4
Fe	0.99	0.10	0.04	−0.01
V	0.99	−0.01	−0.11	0.00
Co	0.99	0.13	−0.04	−0.07
Al	0.98	0.12	−0.07	−0.11
Zr	0.97	−0.09	0.10	0.07
Y	0.97	−0.16	−0.12	0.03
Ni	0.97	0.19	0.04	0.05
Rb	0.97	0.18	−0.04	−0.08
Sc	0.97	0.10	−0.03	−0.02
Ca	−0.96	−0.15	0.19	0.09
Zn	0.96	0.17	0.08	−0.01
CaCO ₃	−0.96	−0.12	−0.08	0.19
Cr	0.95	0.14	−0.06	0.12
P	0.95	0.17	−0.16	0.09
Mn	0.95	−0.21	−0.11	0.15
Ce	0.93	−0.09	0.07	−0.04
Nb	0.90	−0.26	−0.08	0.27
LOI ₅₅₀	0.90	0.03	0.29	0.02
Cu	0.81	0.22	0.27	0.07
S	0.70	0.38	0.38	0.08
Sn	0.68	0.13	0.21	0.05
U	−0.60	0.55	−0.15	0.48
Pb	0.42	0.23	0.30	0.31
Ti	0.33	−0.75	−0.23	0.47
Mo	−0.05	0.72	0.36	0.12
Re	−0.61	0.62	−0.25	0.24
Th	0.53	−0.60	−0.13	0.35
As	−0.53	0.58	−0.52	0.24
Sr	−0.54	−0.32	0.71	0.10
Sb	0.61	0.08	−0.69	−0.25
Eigen value	20.402	3.201	2.108	1.075
% Variance	68.01	10.67	7.03	3.58
Cumulative variance	68.01	78.67	85.70	89.28

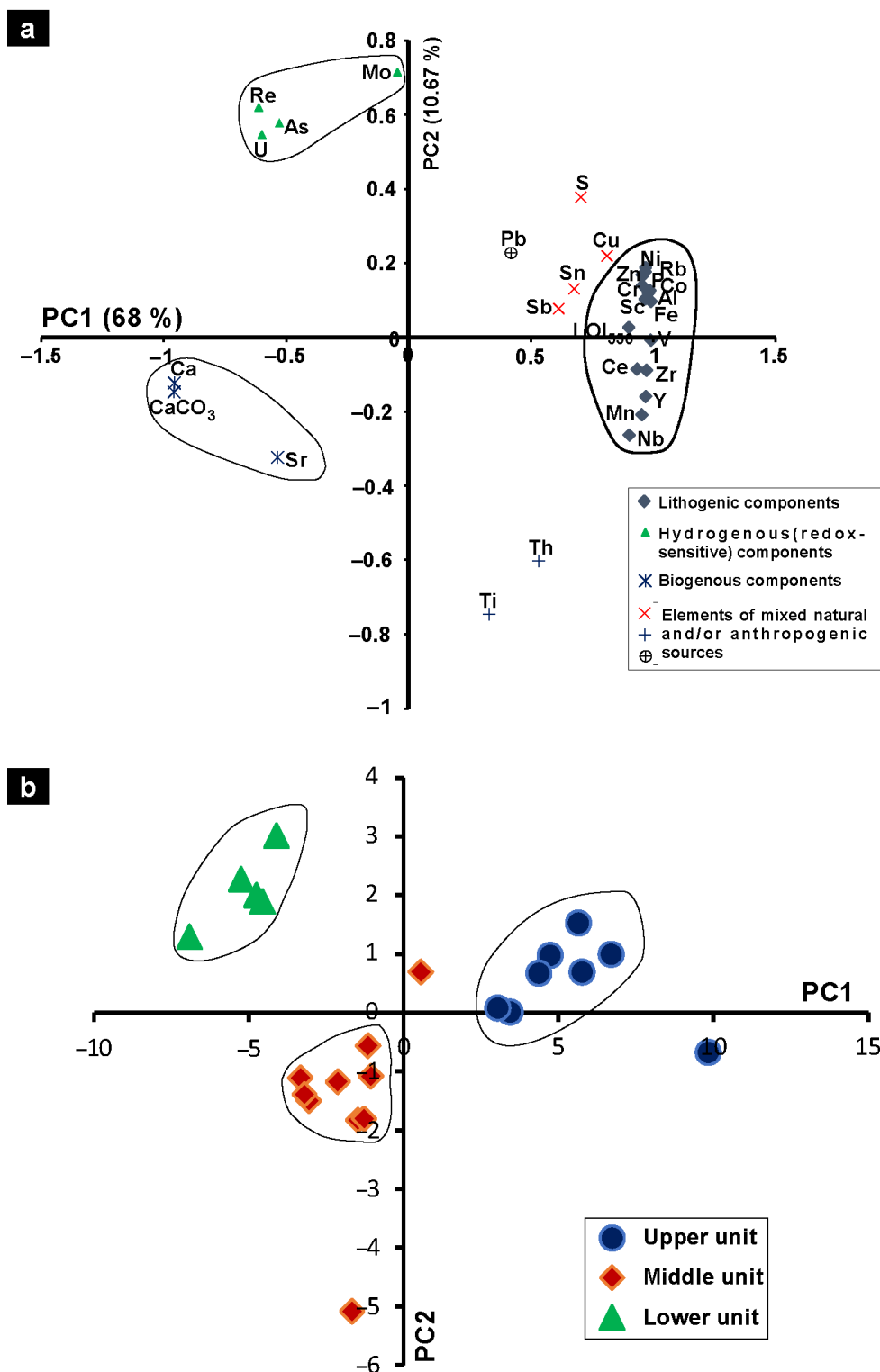


Figure 7. (a) Biplot of PC1 and PC2 (R-mode) loading and clustering of elements (variables) into lithogenic having higher PC1 and PC2 loading, redox-sensitive elements having negative PC1 and positive PC2 values, and carbonate related elements having negative PC1 and PC2 loadings. (b) Biplot of PC1 and PC2 (Q-mode) loading and subdivision of the core into three units. Samples (cases) in the upper unit having high component 1 scores are enriched in lithogenous elements, and other sediments (middle and lower units) are enriched in biogenous and hydrogenous elements.

The plot (Figure 7b) of component scores (Table 4) enabled clustering samples into three major groups, corresponding to the upper, middle, and lower units. Component 1 cluster samples from the upper unit that show positive scores (>1), whereas the samples of the middle and lower units display negative scores. These samples occupy the right upper quadrant and are enriched in the elements of lithogenic origin Al, Fe, Mg, Na, K, P, LOI₅₅₀, Mn, V, Cr, Co, Ni, Zn, Zr, Rb, and Sc. Component 2 characterizes samples from the lower unit that show positive scores (>1). These samples occupy the upper left quadrant and are enriched in Mo, U, As, and Re. The third group of samples occupies the lower left quadrant of the figure and are dominated by carbonate- and biogenous-related elements Ca, CaCO₃, and Sr (Figure 7b). The second and third groups are water derived constituents.

Table 4. Results of principal component (Q-mode) analysis, four components (PC1-PC4) are extracted with the PC1 and PC2 are the most important. Significant values are in bold.

Sample	PC1	PC2	PC3	PC4
SH-1	4.72	0.98	0.09	−1.11
SH-2	9.83	−0.67	−4.35	−0.95
SH-3	3.43	0.02	−0.77	−1.76
SH-4	5.75	0.69	1.65	0.66
SH-5	5.64	1.53	1.91	1.27
SH-6	6.69	1.00	0.32	1.16
SH-7	3.03	0.08	−0.06	0.02
SH-8	4.35	0.68	0.32	0.46
SH-9	0.55	0.70	2.13	0.08
SH-10	−1.16	−0.56	1.83	−0.69
SH-11	−1.06	−1.08	1.58	−0.95
SH-12	−1.48	−1.83	0.99	−1.29
SH-13	−1.28	−1.80	0.87	0.04
SH-14	−3.06	−1.49	−0.02	−0.84
SH-15	−1.67	−5.08	−1.29	2.01
SH-16	−3.33	−1.10	−0.50	−0.69
SH-17	−2.12	−1.17	0.71	0.36
SH-18	−3.21	−1.39	−0.91	1.54
SH-19	−5.25	2.27	−1.00	0.27
SH-20	−4.12	3.02	−1.51	1.34
SH-21	−4.76	2.00	−0.98	−0.37
SH-22	−6.92	1.30	−0.23	−1.24
SH-23	−4.56	1.90	−0.78	0.68

5. Discussion

The components of the shallow subsurface sediments of the coastal creek north of the southern Al-Shuaiba Lagoon consist mainly of lithogenous, organic matter, and water column-derived (hydrogenous and biogenous) constituents. Based on the geochemical data and statistical analysis, three levels of elemental enrichments corresponding to the lower, middle, and upper units of the core can be distinguished. The enriched elements/constituents are different in these levels reflecting the different driving forces and sources. Variations in element concentrations reflect their behaviour in the water column, redox conditions, and the rate of terrigenous and organic matter influx. The significant positive correlation between Al and trace elements (Mn, V, Cr, Co, Ni, Cu, Zn, Rb, Sc,

Zr, Y, and Nb) suggests that these elements are hosted essentially by the lithogenous constituents [42]. Elements of lithogenic origin are enriched in the upper unit. The high organic carbon content in the upper unit is attributed to the high organic matter influx rather than to the depletion of oxygen in the bottom water. A clear downcore depletion in lithogenous elements is apparent below the dark grey upper unit. This depletion is attributed to the general low detrital influx and the significant dilution of the detrital component with biogenic component (CaCO_3). The middle unit is enriched in biogenous constituents such as Sr, Ca, and CaCO_3 [43,44]. The covariation of Sr with Ca indicates that Sr is fixed primarily in the calcareous skeletal material. The most important hydrogenous constituents are Mo, As, U, and Re, which are relatively enriched in the sediments of the lower unit.

The elemental enrichments in the upper and lower units are the most distinctive. Both natural and anthropogenic drivers are responsible for elemental enrichments. To interpret the driving forces for these enrichments it is important to take the climatic setting of the area into account. The area, in general, is extremely hot and arid with no source of terrigenous influx except for aeolian transportation. Along the Red Sea coast, lithogenic elements are supplied from land to the coastal area mainly through wadis and by aeolian transportation [21,45]. However, the area of study is extremely arid and lacks terrigenous influx since the nearby wadis are generally inactive. Noteworthy, the increased enrichment levels of lithogenous elements in the upper part probably coincide with the road construction between the southern and northern Al-Shuaiba Lagoons. Therefore, this enrichment is induced by human activities particularly by landfills during road construction and the subsequent road runoff. Ghandour et al. [7] recorded a level of enrichment of geogenic elements in the southern nearshore zone area of Sharm Obhur, Jeddah, and they attributed this enrichment to dumping and landfills. The slight enrichment of Cu, Zn, and Pb in the upper part may be related to anthropogenic activities such as atmospheric fallout from the fuel combustion or rare boat activity.

The second most distinct enrichment level is recorded for elements Mo, As, U, and Re from the lower unit. They covary in the core suggesting that they have had a similar mechanism of precipitation. They are easily reduced and precipitated from anoxic bottom water [42,46] and, therefore, they are enriched in the much more restricted O_2 -deficient setting [47]. Both natural and anthropogenic drivers can be responsible for oxygen depletion. However, this event precedes the beginning of anthropo-pressure. Oxygen decline is related to a lack of oxygen supply due to density stratification. High-temperature anomalies lead to water column stratification and the development of bottom anoxia in this shallow water. In such a setting, a solar heating-induced density gradient within the water column and water stratification prevents efficient mixing. In addition, warming reduces the solubility of oxygen in the water and enhances microbial activity. The warming effect tends to be severe in semi-enclosed basins. Abundant *Sorites orbiculus*, high palaeo-tidal elevation, and enrichments in both $\delta^{18}\text{O}$ and $\delta^{13}\text{C}$ values in the shallow subsurface coastal sediments at Al-Shuaiba during the AD 1000–1550 interval were attributed to the Medieval climate anomaly (MCA) warming event [30,48]. The MCA was a period of climate perturbation during which the Earth's temperature was similar to or slightly higher than the temperature of the 20th century [49]. The key drivers for this warming event include solar activity, ocean cycles, aerosols from volcanic eruptions, and greenhouse gases [48–52].

Redox-Sensitive Elements

Trace metal enrichment and trace metal ratios in the lagoonal and ocean bottom sediments have been used to address paleoredox conditions [53–58]. Molybdenum (Mo), V, Cr, Co, Ni, Cu, Zn, As, U, and Re are currently of high interest in this regard since they are reduced to a lower valency and become reactive or insoluble under anoxic conditions [54]. The trace elements in the core sediments include both hydrogenous and lithogenous components. To use trace elements as paleoredox proxy, it is important first to determine whether the elements are hydrogenous or lithogenous. A significant positive correlation

between Al and trace elements indicates that the element is contained in the terrigenous component. In the present study, Al displays moderate to low correlation with Mo ($r < 0.3$) and negative correlation with U, As, and Re suggesting that these elements are of authigenic origin, and they are reliable paleoredox proxies. Hydrogenous elements are the ones that can be used for paleoenvironmental interpretations. Multi-elements proxies are more suitable for the analysis of paleo-redox conditions rather than a single elemental proxy [58]. Mo, As, Re, and U concentrations and their Al-normalized values show positive shifts in the lower unit, whereas no such positive shifts were observed for other elements. This suggests that the creek has experienced suboxic/anoxic bottom water conditions during the deposition of the lower unit. Enrichments in Re, Mo, As, and U are well known for numerous Phanerozoic organic-rich shales and their enrichment is usually associated with anoxic to euxinic bottom-water conditions [59–61]. The lithogenic origin of elements V, Cr, Co, Ni, Cu, and Zn obliterates their significances as reliable paleoredox indicators. The low concentrations and low Al-normalized, as well as EF values for these elements in the lower unit, may be explained by the “basin reservoir effect” [62]. This effect suggests that the concentrations of these elements decreased under an increasingly stagnant bottom water body due to their removal to the sediment without adequate resupply by water renewal. The depletion of Mn in the lower unit suggests that under anoxic conditions Mn occurs as Mn (II) in the dissolved phase [54]. The high solubility of Mn^{2+} in sediments deposited under reducing conditions may result in Mn being depleted if fixation in carbonate minerals is not possible [63].

The results presented in this study so far show that it is possible to distinguish clearly between anoxic and oxic depositional conditions for the shallow subsurface coastal sediments of the northern Al-Shuaiba Lagoon. The study helps in understanding the process of shallow water hypoxia and the most relevant redox sensitive elements.

6. Conclusions

The present study investigates the elemental enrichments and interprets them in the context of redox bottom conditions and increased terrigenous influx. The chemical data from the shallow subsurface sediments of the coastal creek that was connecting the southern and northern Al-Shuaiba Lagoons reflect environmental changes through time either due to natural and/or anthropogenic influences.

1. Based on the colour of sediments, vertical variation in elemental concentrations, and statistical analysis, the core was subdivided into three units, upper, middle, and lower.
2. The upper organic-rich unit shows enrichment of lithogenous elements and values of LOI_{550} (organic matter) content. Trace elements Mn, V, Cr, Co, Ni, and Zn display significant positive correlations with Al suggesting their lithogenic source. Though these elements are derived from a lithogenic source, their enrichment is related to human activity. This level is attributed to the road construction between the two lagoons. The relatively high concentrations of Pb and Cu in the upper unit are possibly related to atmospheric road dust and from the increasing movement of cars. Though the road construction limited the water circulation between the two lagoons, the sediments were deposited under oxic conditions as shown by the depletion of redox-sensitive elements.
3. The lower and middle units of the core contain relatively higher carbonate content than the upper part. Strontium (Sr) distribution appears to be controlled by the presence of biogenic carbonate minerals. Calcium (Ca) distribution follows largely the spatial distribution of the carbonate content since Ca, Sr, and $CaCO_3$ are biogenic components.
4. The chemical composition of the lower unit suggests deposition in poorly circulated bottom water, with prevailing suboxic or even anoxic conditions probably related to the solar forcing (Medieval climate anomaly). This is confirmed by depletions in Mn and Co and relative enrichment of Mo, As, U, and Re. The distribution pattern of the Al-normalized redox sensitive elements is characterized by markedly high values

in the lower unit. They display a negative to poor correlation with Al excluding lithogenic sources. Molybdenum (Mo), As, U, and Re are reliable and most promise proxies for redox conditions since they behave conservatively in oxygenated waters and are enriched in anoxic sediments.

Author Contributions: I.M.G., proposal of the idea, conceptualization, sample collection and coordination for analysis, data analysis, and writing the manuscript; M.H.A., data analysis, reviewing the manuscript and participation in the discussion. All authors have read and agreed to the published version of the manuscript.

Funding: This project was funded by the Deanship of Scientific Research (DSR) at King Abdulaziz University, Jeddah, under grant No. G: 617-150-1441.

Data Availability Statement: The data are available upon request at KAU and can be requested by contacting the corresponding author.

Acknowledgments: The authors thank the DSR for this technical and financial support. The authors are grateful to Aaid Al-Zubairi (KAU) for his assistance in the fieldwork. The authors would like to thank Brian Jones (Wollongong Univ.) for his constructive comments and suggestions that improved the manuscript. We are very grateful to the editor and the reviewers for their constructive comments and editorial handling.

Conflicts of Interest: The authors declare no conflict of interest.

References

1. Danovaro, R. Pollution threats in the Mediterranean Sea: An overview. *Chem. Ecol.* **2003**, *19*, 15–32. [[CrossRef](#)]
2. Barbier, E.B.; Hacker, S.D.; Kennedy, C.; Koch, E.W.; Stier, A.C.; Silliman, B.R. The value of estuarine and coastal ecosystem services. *Ecol. Monogr.* **2011**, *81*, 169–193. [[CrossRef](#)]
3. Robb, C.K. Assessing the impact of human activities on British Columbia's estuaries. *PLoS ONE* **2014**, *9*, e99578. [[CrossRef](#)]
4. Coynel, A.; Gorse, L.; Curti, C.; Schafer, J.; Grosbois, C.; Morelli, G.; Ducassou, E.; Blanc, G.; Maillet, G.M.; Mojtabid, M. Spatial distribution of trace elements in the surface sediments of a major European estuary (Loire Estuary, France): Source identification and evaluation of anthropogenic contribution. *J. Sea Res.* **2016**, *18*, 77–91. [[CrossRef](#)]
5. Badassan, T.E.; Avumadi, A.M.; Ouro-Sama, K.; Gnandi, K.; Jean-Dupuy, S.; Probst, J.L. Geochemical Composition of the Lomé Lagoon Sediments, Togo: Seasonal and Spatial Variations of Major, Trace and Rare Earth Element Concentrations. *Water* **2020**, *11*, 3026. [[CrossRef](#)]
6. McAlister, J.J.; Smith, B.J.; Neto, J.B.; Simpson, J.K. Geochemical distribution and bioavailability of heavy metals and oxalate in street sediments from Rio de Janeiro, Brazil: A preliminary investigation. *Environ. Geochem. Health* **2005**, *5*, 429–441. [[CrossRef](#)]
7. Ghandour, I.M.; Basaham, S.; Al-Washmi, A.; Masuda, H. Natural and anthropogenic controls on sediment composition of an arid coastal environment: Sharm Obhur, Red Sea, Saudi Arabia. *Environ. Monit. Assess* **2014**, *3*, 1465–1484. [[CrossRef](#)] [[PubMed](#)]
8. Weeks, S.J.; Currie, B.; Bakun, A. Massive emissions of toxic gas in the Atlantic. *Nature* **2002**, *415*, 493–494. [[CrossRef](#)] [[PubMed](#)]
9. Morina, A.; Morina, F.; Djikanović, V.; Spasić, S.; Krpo-Četković, J.; Kostić, B.; Lenhardt, M. Common barbel (*Barbus barbus*) as a bioindicator of surface river sediment pollution with Cu and Zn in three rivers of the Danube River Basin in Serbia. *Environ. Sci. Pollut. Res.* **2016**, *23*, 6723–6734. [[CrossRef](#)] [[PubMed](#)]
10. Schintu, M.; Marrucci, A.; Marras, B.; Galgani, F.; Buosi, C.; Ibba, A.; Cherchi, A. Heavy metal accumulation in surface sediments at the port of Cagliari (Sardinia, western Mediterranean): Environmental assessment using sequential extractions and benthic foraminifera. *Mar. Pollut. Bull.* **2016**, *111*, 45–56. [[CrossRef](#)] [[PubMed](#)]
11. Shi, Z.; Wang, X.; Ni, S. Metal contamination in sediment of one of the upper reaches of the Yangtze River: Mianyuan River in Longmenshan region, Southwest of China. *Soil Sediment Contam.* **2015**, *24*, 368–385. [[CrossRef](#)]
12. Wang, X.; Shi, Z.; Shi, Y.; Ni, S.; Wang, R.; Xu, W.; Xu, J. Distribution of potentially toxic elements in sediment of the Anning River near the REE and V-Ti magnetite mines in the Panxi Rift, SW China. *J. Geochem. Explor.* **2018**, *184*, 110–118. [[CrossRef](#)]
13. Al-Rousan, S.; Al-Taani, A.A.; Rashdan, M. Effects of pollution on the geochemical properties of marine sediments across the fringing reef of Aqaba, Red Sea. *Mar. Pollut. Bull.* **2016**, *110*, 546–554. [[CrossRef](#)]
14. Krishnakumar, S.; Ramasamy, S.; Chandrasekar, N.; Peter, T.S.; Gopal, V.; Godson, P.S.; Magesh, N.S. Trace element concentrations in reef associated sediments of Koswari Island, Gulf of Mannar biosphere reserve, southeast coast of India. *Mar. Pollut. Bull.* **2017**, *117*, 515–522. [[CrossRef](#)] [[PubMed](#)]
15. Bonanno, G.; Di Martino, V. Trace element compartmentation in the seagrass *Posidonia oceanica* and biomonitoring applications. *Mar. Pollut. Bull.* **2017**, *116*, 196–203. [[CrossRef](#)] [[PubMed](#)]
16. Ternengo, S.; Marengo, M.; El Idrissi, O.; Yepka, J.; Pasqualini, V.; Gobert, S. Spatial variations in trace element concentrations of the sea urchin, *Paracentrotus lividus*, a first reference study in the Mediterranean Sea. *Mar. Pollut. Bull.* **2018**, *129*, 293–298. [[CrossRef](#)]

17. Zhang, H.; Walker, T.R.; Davis, E.; Ma, G. Spatiotemporal characterization of metals in small craft harbour sediments in Nova Scotia, Canada. *Mar. Pollut. Bull.* **2019**, *140*, 493–502. [[CrossRef](#)]
18. Vinodhini, R.; Narayanan, M. Bioaccumulation of heavy metals in organs of fresh water fish *Cyprinus carpio* (Common carp). *Int. J. Environ. Sci. Technol.* **2008**, *5*, 179–182. [[CrossRef](#)]
19. Badr, N.B.; El-Fiky, A.A.; Mostafa, A.R.; Al-Mur, B.A. Metal pollution records in core sediments of some Red Sea coastal areas, Kingdom of Saudi Arabia. *Environ. Monit. Assess* **2009**, *155*, 509–526. [[CrossRef](#)]
20. Ma, L.; Wu, J.; Abuduwaili, J.; Liu, W. Geochemical responses to anthropogenic and natural influences in Ebinur Lake sediments of arid Northwest China. *PLoS ONE* **2016**, *11*, e0155819. [[CrossRef](#)]
21. Rasul, N.M. Lagoon sediments of the Eastern Red Sea: Distribution processes, pathways and patterns. In *The Red Sea*; Springer: Berlin/Heidelberg, Germany, 2015; pp. 281–316.
22. Al-Washmi, H.A.; Gheith, A.M. Recognition of diagenetic dolomite and chemical surface features of the quartz grains in coastal sabkha sediments of the hypersaline Shuaiba Lagoon, Eastern Red Sea Coast, Saudi Arabia. *J. King Abdulaziz Univ. Mar. Sci.* **2003**, *14*, 101–112. [[CrossRef](#)]
23. Basaham, A.S. Mineralogical and chemical composition of the mud fraction from the surface sediments of Al-Kharrar, a Red Sea coastal lagoon. *Oceanologia* **2008**, *50*, 557–575.
24. Abu-Zied, R.H.; Bantan, R.A. Hypersaline benthic foraminifera from the Shuaiba Lagoon, eastern Red Sea, Saudi Arabia: Their environmental controls and usefulness in sea-level reconstruction. *Mar. Micropaleontology* **2013**, *103*, 51–67. [[CrossRef](#)]
25. Basaham, A.S.; El Sayed, M.A.; Ghandour, I.M.; Masuda, H. Geochemical background for the Saudi Red Sea coastal systems and its implication for future environmental monitoring and assessment. *Environ. Earth Sci.* **2015**, *74*, 4561–4570. [[CrossRef](#)]
26. Basaham, A.S.; Ghandour, I.M.; Haredy, R. Controlling factors on the geochemistry of Al-Shuaiba and Al-Mejarma coastal lagoons, Red Sea, Saudi Arabia. *Open Geosci.* **2019**, *11*, 426–439. [[CrossRef](#)]
27. Youssef, M.; El-Sorogy, A. Environmental assessment of heavy metal contamination in bottom sediments of Al-Kharrar lagoon, Rabigh, Red Sea, Saudi Arabia. *Arab. J. Geosci.* **2016**, *9*, 474. [[CrossRef](#)]
28. Ahmed, F.C.; Sultan, S.A.R. The effect of meteorological forcing on the flushing of Shuaiba Lagoon on the eastern coast of the Red Sea. *J. King Abdulaziz Univ. Mar. Sci.* **1992**, *3*, 3–9. [[CrossRef](#)]
29. Al-Barakati, A.M.A. Application of 2-D tidal model, Shuaiba Lagoon, eastern Red Sea coast. *Can. J. Comput. Math. Nat. Sci. Med.* **2010**, *1*, 9–20.
30. Abu-Zied, R.H.; Bantan, R.A. Palaeoenvironment, palaeoclimate and sea-level changes in the Shuaiba Lagoon during the late Holocene (last 3.6 ka), eastern Red Sea coast, Saudi Arabia. *Holocene* **2015**, *25*, 1301–1312. [[CrossRef](#)]
31. Al-Farawati, R.; El Sayed, M.; Shaban, Y.; El-Maradney, A.; Orif, M. Phosphorus Speciation in the Coastal Sediments of Khawr Ash Shaibah Al-Masdudah: Coastal Lagoon in the Eastern Red Sea, Kingdom of Saudi Arabia. *Arab Gulf J. Sci. Res.* **2014**, *32*, 93–101.
32. Braithwaite, C.J.R. Geology and paleogeography of the Red Sea region. In *Key Environments: Red Sea*; Edwards, A.J., Mead, S.M., Eds.; Pergamon Press: New York, NY, USA, 1987; pp. 22–24.
33. Brown, G.F.; Schimdt, D.L.; Huffman, A.C. *Shield Area of Western Saudi Arabia, Geology of the Arabian Peninsula*; Professional Paper 560-A; US Geological Survey: Reston, VA, USA, 1989.
34. Hötzl, H.; Zötl, J.G. Climatic changes during the Quaternary Period. In *Quaternary Period in Saudi Arabia*; Al-Sayari, S.S., Zötl, J.G., Eds.; Springer: New York, NY, USA, 1978; pp. 301–311.
35. Sofianos, S.S.; Johns, W.E.; Murray, S.P. Heat and freshwater budgets in the Red Sea from direct observations at Bab el Mandeb. *Deep Sea Research Part II: Top. Stud. Oceanogr.* **2002**, *49*, 1323–1340. [[CrossRef](#)]
36. Abu-Zied, R.H.; Bantan, R.A.; El Mamoney, M.H. Present environmental status of the Shuaiba Lagoon, Red Sea Coast, Saudi Arabia. *J. King Abdulaziz Univ. Mar. Sci.* **2011**, *22*, 159–179. [[CrossRef](#)]
37. Heiri, O.; Lotter, A.F.; Lemcke, G. Loss-on-ignition as a method for estimating organic and carbonate content in sediments: Reproducibility and comparability of results. *J. Paleolimnol.* **2001**, *25*, 101–110. [[CrossRef](#)]
38. Chester, R.; Stoner, J.H. Pb in particulates from the lower atmosphere of the eastern Atlantic. *Nature* **1973**, *245*, 27–28. [[CrossRef](#)]
39. Zhang, J.; Liu, C.L. Riverine composition and estuarine geochemistry of particulate metals in China—Weathering features, anthropogenic impact and chemical fluxes estuarine. *Coast. Shelf Sci.* **2002**, *54*, 1051–1070. [[CrossRef](#)]
40. Tribovillard, N.P.; Desprairies, A.; Lallier-Vergès, E.; Bertrand, P.; Moureau, N.; Ramdani, A.; Ramanampisoa, L. Geochemical study of organic-matter rich cycles from the Kimmeridge Clay Formation of Yorkshire (UK): Productivity versus anoxia. *Palaeogeogr. Palaeoclimatol. Palaeoecol.* **1994**, *108*, 165–181. [[CrossRef](#)]
41. Murphy, A.E.; Sageman, B.B.; Hollander, D.J.; Lyons, T.W.; Brett, C.E. Black shale deposition and faunal overturn in the Devonian Appalachian basin: Clastic starvation, seasonal water-column mixing, and efficient biolimiting nutrient recycling. *Paleoceanography* **2000**, *15*, 280–291. [[CrossRef](#)]
42. Hild, E.; Brumsack, H.-J. Major and minor element geochemistry of Lower Aptian sediments from the NW German Basin (core Hoheneggelsen KB 40). *Cretac. Res.* **1998**, *19*, 615–633. [[CrossRef](#)]
43. Whitfield, M. Interactions between Phytoplankton and Trace Metals in the Ocean-Introduction. *Adv. Mar. Biol.* **2001**, *41*, 3–130.
44. Ho, T.Y.; Quigg, A.; Finkel, Z.V.; Milligan, A.J.; Wyman, K.; Falkowski, P.G.; Morel, F.M. The elemental composition of some marine phytoplankton 1. *J. Phycol.* **2003**, *39*, 1145–1159. [[CrossRef](#)]

45. Haredy, R.; Ghandour, I.M. Geochemistry and mineralogy of the shallow subsurface Red Sea coastal sediments, Rabigh, Saudi Arabia: Provenance and paleoenvironmental implications. *Turk. J. Earth Sci.* **2020**, *29*, 257–279. [[CrossRef](#)]
46. Landing, W.M.; Lewis, B.L. Collection, processing, and analysis of marine particulate and colloidal material for transition metals. In *Marine Particles: Analysis and Characterization*; Hurd, D.C., Spencer, D.W., Eds.; American Geophysical Union Geophysical Monograph Series; American Geophysical Union: Washington, DC, USA, 1991; Volume 63, pp. 263–272.
47. Lézin, C.; Andreu, B.; Pellenard, P.; Bouchez, J.L.; Emmanuel, L.; Fauré, P.; Landrein, P. Geochemical disturbance and paleoenvironmental changes during the Early Toarcian in NW Europe. *Chem. Geol.* **2013**, *341*, 1–5. [[CrossRef](#)]
48. Lüning, S.; Gałka, M.; Vahrenholt, F. Warming and cooling: The Medieval Climate Anomaly in Africa and Arabia. *Paleoceanography* **2017**, *32*, 1219–1235. [[CrossRef](#)]
49. Diaz, H.; Trigo, R.; Hughes, M.; Mann, M.; Xoplaki, E.; Barriopedro, D. Spatial and Temporal Characteristics of Climate in Medieval Times Revisited. *Bull. Am. Meteorol. Soc.* **2011**, *92*, 1487–1500. [[CrossRef](#)]
50. Moberg, A.; Sonechkin, D.M.; Holmgren, K.; Datsenko, N.M.; Karlén, W.; Lauritzen, S.-E. Highly variable Northern Hemisphere temperatures reconstructed from low- and high-resolution proxy data. *Nature* **2005**, *433*, 613–617. [[CrossRef](#)]
51. Zhou, L.; Tinsley, B.; Huang, J. Effects on winter circulation of short- and long-term solar wind changes. *Adv. Space Res.* **2014**, *54*, 2478–2490. [[CrossRef](#)]
52. Andrews, M.B.; Knight, J.R.; Gray, L.J. A simulated lagged response of the North Atlantic Oscillation to the solar cycle over the period 1960–2009. *Environ. Res. Lett.* **2015**, *10*, 054022. [[CrossRef](#)]
53. Wignall, P.B.; Meyers, K.J. Interpreting benthic oxygen levels in mudrocks: A new approach. *Geology* **1988**, *16*, 452–455. [[CrossRef](#)]
54. Calvert, S.E.; Pedersen, T.F. Geochemistry of Recent oxic and anoxic marine sediments: Implications for the geological record. *Mar. Geol.* **1993**, *113*, 67–88. [[CrossRef](#)]
55. Morford, J.L.; Emerson, S. The geochemistry of redox sensitive trace metals in sediments. *Geochim. Cosmochim. Acta* **1999**, *63*, 1735–1750. [[CrossRef](#)]
56. Algeo, T.J.; Maynard, J.B. Trace-element behavior and redox facies in core shales of Upper Pennsylvanian Kansas-type cyclothems. *Chem. Geol.* **2004**, *206*, 289–318. [[CrossRef](#)]
57. Rimmer, S.M.; Thompson, J.; Goodnight, S.; Robl, T.L. Multiple controls on the preservation of organic matter in Devonian–Mississippian marine black shales: Geochemical and petrographic evidence. *Palaeogeogr. Palaeoclimatol. Palaeoecol.* **2004**, *215*, 125–154. [[CrossRef](#)]
58. Tribouvillard, N.; Algeo, T.J.; Lyons, T.; Riboulleau, A. Trace metals as paleoredox and paleoproductivity proxies: An update. *Chem. Geol.* **2006**, *232*, 12–32. [[CrossRef](#)]
59. Brumsack, H.-J. The trace metal content of recent organic carbon-rich sediments: Implications for Cretaceous black shale formation. *Palaeogeogr. Palaeoclimatol. Palaeoecol.* **2006**, *232*, 344–361. [[CrossRef](#)]
60. Warning, B.; Brumsack, H.-J. Trace metal signatures of eastern Mediterranean sapropels. *Palaeogeogr. Palaeoclimatol. Palaeoecol.* **2000**, *158*, 293–309. [[CrossRef](#)]
61. Wilde, P.; Lyons, T.W.; Quinby-Hunt, M.S. Organic carbon proxies in black shales: Molybdenum. *Chem. Geol.* **2004**, *206*, 167–176. [[CrossRef](#)]
62. Algeo, T.J.; Lyons, T.W. Mo-total organic carbon covariation in modern anoxic marine environments: Implications for analysis of paleoredox and paleohydrographic conditions. *Paleoceanography* **2006**, *21*, PA1016. [[CrossRef](#)]
63. Scholz, F.; McManus, J.; Sommer, S. The manganese and iron shuttle in a modern euxinic basin and implications for molybdenum cycling at euxinic ocean margins. *Chem. Geol.* **2013**, *355*, 56–68. [[CrossRef](#)]